Microchimica Acta (2019) 186: 456
https://doi.org/10.1007/s00604-019-3366-0

CORRECTION

Correction to: Magnetic-core@dual-functional-shell nanocomposites with peroxidase mimicking properties for use in colorimetric and electrochemical sensing of hydrogen peroxide

Yuqing Li[1] · Jing Liu[2] · Yingchun Fu[1] · Qingji Xie[2] · Yanbin Li[1,3]

Published online: 18 June 2019

Abstract

A self-sacrificing catalytic method is described for the preparation of magnetic core/dual-functional-shell nanocomposites composed of magnetite, gold and Prussian blue (type Fe_3O_4@Au-PB). Two reaction pathways are integrated. The first involves chemical dissolution of Fe_3O_4 (the self-sacrificing step) by acid to release ferrous ions which then reacts with hexacyanoferrate(IV) to generate PB in the proximity of the magntic nanoparticles (MNPs). The second involves the reduction of tetrachloroaurate by hydroxylamine to generate gold under the catalytic effect of the MNPs. At the end, the MNP@Au-PB nanocomposite is formed. This method exploits both the chemical reactivity and catalytic effect of the MNPs in a single step. The multi-function material was applied (a) in an optical assay for H_2O_2; (b) in an amperometric assay for H_2O_2; (c) in an enzymatic choline assay using immobilized choline oxidase. The limit of electrochemical detection of H_2O_2 (at a potential as low as 50 mV) is 1.1 μM which is comparable or better than most analogous methods. The sensors display superior performance compared to the use of conventional core@single-shell (MNP@Au-PB) nanomaterials.

Keywords Magnetic nanoparticles · Core@shell nanocomposites · Self-sacrifice · Peroxidase-mimetic · Electrochemical catalysis · Colorimetry · Sensor · H_2O_2 · Glucose · Choline oxidase

Introduction

Magnetic nanocomposites, integrating unique magnetic properties/functions and desired functions from other components, have drawn increasing attractions and have been applied in various fields [1–5]. Plenty of preparation methods have been developed to meet various requirements. Due to abundant surface properties of magnetic materials, it is readily to introduce/modify other components onto the surface of magnetic core and form functional shell(s) [6–21]. The exposed shell makes itself sensitive and reactive to the surroundings, thus realizes applications such as sensing [6, 7, 10, 11, 16], adsorption [12, 13], catalysis [14, 15], therapy [9], and so on. On the other hand, the shell cooperates with the magnetic core, even generates synergistic effect [9, 12, 13]. Currently, the construction of single (functional) layer of shell is well established [6–10]. On the other hand, multiple layers of shells have to be elaborated for multiple extraneous functions [22–25]. The introduction of multiple shells, however, makes the preparation complicated and time consuming. It also brings about other deficiencies such as the unstable linking between layers and the spatial separation of magnetic core from the outer shell. Therefore, methods that can introduce

Yuqing Li and Jing Liu contributed equally to this work.

The online version has been available; however, the corrections that have been suggested in a separate file apart from e.proofing were not carried out. Given here is the corrected article.

The online version of the original article can be found at https://doi.org/10.1007/s00604-018-3116-8

Electronic supplementary material The online version of this article (https://doi.org/10.1007/s00604-019-3366-0) contains supplementary material, which is available to authorized users.

✉ Yingchun Fu
ycfu@zju.edu.cn

[1] College of Biosystems Engineering and Food Science, Zhejiang University, Hangzhou 310058, China

[2] Key Laboratory of Chemical Biology and Traditional Chinese Medicine Research (Ministry of Education of China), Hunan Normal University, Changsha 410081, China

[3] Department of Biological and Agricultural Engineering, University of Arkansas, Fayetteville, AR 72701, USA

layer of shell with multiple components/functions should flourish the branches of magnetic nanocomposites and lead to new applications.

Owning to the abundant properties of ferrous elements and their compounds, plenty of strategies have been developed for the modification of outer layers (shells) to magnetic nanomaterials, mainly including physical and chemical ways [1, 3–5]. Recently, a sacrificing method was also explored with characteristics of supplying reactants of shell from the sacrificing of magnetic nanomaterials themselves through chemical/electrochemical ways [7, 9, 10]. Briefly, ferrous components in magnetic nanomaterials release ferrous ions in acidic solution, followed by the formation of new shell via the reaction between the released ferrous ions with other co-existing reactants. For example, recently our group developed a new electrochemical method to converse magnetic nanoparticles (MNPs) to Prussian blue (PB) [7]. By applying a high-potential on the gold electrode, water can be split into gaseous oxygen and hydrogen ions, which reacted with MNPs (Fe_3O_4) to release ferrous ions. Then in a low-potential process, ferrous ions reacted with co-existing $Fe(CN)_6^{4-}$ ions to form PB. The sacrificing methods presented unique proximity effect, namely, confining the reactions occurred on the surface of magnetic nanomaterials. Moreover, the formed shell shares same ferrous components with magnetic nanomaterials, gifting high stability of the core@shell structure. However, current researches exploited the sacrificing method for the generation of sole-component shell, leaving the methods for the preparation of multiple-component shell rarely exploited [7, 9, 10]. Furthermore, the shell generated from the sacrificing method is PB analogues. As well known, PB analogues are with high catalysis ability and even the peroxidase-like activity, however, the lack of chemical groups on the surface inhibits further functionalization [26], so complicated procedures are required to introduce other species onto PB surface [27–29]. This significantly limits potential of applications. Therefore, by integrating the unique advantages of sacrificing method with other properties/functions of magnetic nanomaterials, it remains vast space and impetus to exploit new method to extend the modification/functionalization of magnetic nanomaterials to fulfill diversified requirements of applications.

A self-sacrificing-catalyzing method is proposed to prepare MNP@Au-PB core@dual-functional-shell nanocomposites for sensing applications. Owning to the wide presence of H_2O_2 in natural environmental and applications in industrial fields and biological study, efficient detection of H_2O_2 is of high importance [30–33]. Therefore, electrochemical and colorimetric sensors for H_2O_2 were developed using the new nanocomposites. Briefly as shown in Scheme 1, HCl, $K_4Fe(CN)_6$, $HAuCl_4$ and NH_2OH are added to the suspension of Fe_3O_4, in which there are two paths of chemical reactions occurred. The first one is that HCl reacts to Fe_3O_4 to release

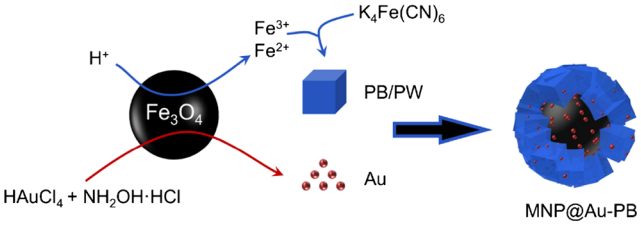

Scheme 1 Illustration of the preparation of MNP@Au-PB nanocomposites

ferrous ions (Fe^{3+} and Fe^{2+}), which then react to coexisting $K_4Fe(CN)_6$ to generate PB and Prussian white (PW, analogue of PB, classified as PB in convenience below) in the proximity of MNPs. The second one is the reduction of $HAuCl_4$ by NH_2OH to generate Au nanoparticles triggered by the catalysis effect of MNPs. Finally, the nanocomposites with MNPs as the core and with Au-PB as the dual-functional-shell are yielded. This method takes advantages of the chemical reactivity and catalysis effect of MNPs, generates the dual-functional-shell composites in a one-pot and one-step way. Three state-of-art sensing applications were further studied by exploring the multi-function deriving from the shell. Digital inspection, electrochemical methods, scanning electron microscopy (SEM), transmission electron microscope (TEM), Fourier transform infrared spectroscopy (FTIR), and X-ray photoelectron spectroscopy (XPS) were employed to characterize the morphology, constituent, electrochemical and catalytic properties of the composites. The yielded dual-functional-shell nanocomposites presented higher catalysis activity to H_2O_2 and higher immobilization amount of choline oxidase (ChOx) comparing with the analogues with single-shell. Electrochemical and colorimetric sensing and biosensing platforms were further developed based on these performances. The method might bring new insight for the preparation of multi-functional magnetic composites for diversified applications.

Experimental section

Materials and apparatus Fe_3O_4 MNPs were purchased from Aladdin Bio-Chem Technology Co., LTD (Shanghai, China, www.aladdin-e.com). Hydrogen peroxide (H_2O_2, 30%), sulfuric acid (H_2SO_4, assay NLT 98.0%), hydrochloric acid (HCl, assay NLT 36.0%), potassium ferricyanide ($K_3Fe(CN)_6$), potassium ferrocyanide ($K_4Fe(CN)_6$), ferrous sulfate ($FeSO_4$), hydroxylamine hydrochloride ($NH_2OH{\cdot}HCl$), chloroauric acid ($HAuCl_4$) and sodium citrate ($Na_3C_6H_5O_7$) were purchased from Shanghai Chemical Reagent Co. (Shanghai, China, www.reagent.com.cn). ChOx and choline chloride were purchased from Sigma-Aldrich (St. Louis, MO, USA, www.sigmaaldrich.com). N-(Sulfopropyl)-3,3′,5,5-tetramethylbenzidine, sodium salt

(TMB-PS), L-Cysteine, L-Aspartic acid, L-Glycine and L-Proline were purchased from Sangon Biotech. (Shanghai, China, www.sangon.com). Phosphate buffer (0.1 M, pH = 6.0, 0.1 M K_2HPO_4/KH_2PO_4 + 0.1 M K_2SO_4) was adopted for sensing. All chemicals were of analytical grade or better quality. Milli-Q (Millipore, ≥18 MΩ cm) ultra-pure water was used throughout. All experiments were conducted at room temperature (25 °C).

All electrochemical experiments were conducted on a CHI660E electrochemical workstation (CH Instrument Co., China, www.chinstr.com) with a conventional three-electrode electrolytic cell. The Au electrode with 2.0-mm diameter served as the working electrode, a KCl-saturated calomel electrode (SCE) as the reference electrode, and a carbon rod as the counter electrode. All potentials reported here are cited versus SCE. The FT-IR spectrophotometry, SEM images, TEM images and UV-vis spectrophotometry were collected in a JASCO-4100 Fourier transform infrared spectrometer (Nicolet Instrument Co., Madison, www.thermofisher.com), SU-8010 (Hitachi, Japan, www.hitachi.com) scanning electronic microscope, JEOL JEM-1200EX transmission electron microscope (Hitachi, Japan, www.hitachi.com) and Agilent 8453 UV-vis spectrophotometer (Agilent, USA, www.agilent.com), respectively.

Preparation of MNP@Au-PB, MNP@PB and PB For the typical preparation of MNP@Au-PB, 4 μL of HCl (1 M), 50 μL of $HAuCl_4$ (1 mM), 50 μL of $NH_2OH{\cdot}HCl$ (0.1 M) and 50 μL of $K_4Fe(CN)_6$ (10 mM) were added to 150 μL of MNPs suspension (0.5 mg mL^{-1}) in sequence. After 10 min, the yielded black-blue suspension was washed with dilute hydrochloric acid (pH = 6.0) for three times assisted by magnetic separation and was finally dispersed in 0.1 M phosphate buffer (pH = 6.0).

The preparation of MNP@PB was similar to that for the MNP@Au-PB except the addition of $NaAuCl_4$ and $NH_2OH{\cdot}HCl$. For the preparation of PB thin film, a typical electrochemical deposition method was adopted according to literature [34].

Electrochemical detection of H_2O_2 Firstly, 2 μL of MNP@Au-PB suspension was dropped on the surface of Au electrode. By placing a magnet under the electrode, the MNP@Au-PB composites were anchored on the electrode for further characterization and detection. The characterization of the presence of PB and Au was conducted using CV in a mixture solution containing 0.1 M H_2SO_4 and 0.1 M K_2SO_4 and a solution of 0.05 M H_2SO_4, respectively. Potentiostatic measurements at −0.05 V were adopted for the electrochemical detection of H_2O_2 in 0.1 M phosphate buffer (pH 6.0). Briefly, H_2O_2 stock solutions of different concentrations were successively added to the stirred phosphate buffer, and the differences between currents before and after each addition of H_2O_2 were adopted as response signals.

Optical detection of H_2O_2 Firstly, 30 μL of TMB (10 mM) and 30 μL of H_2O_2 of different concentrations were added into 30 μL of MNP@Au-PB suspensions and kept for 10 min at room temperature for reaction, followed by the addition of 10 μL of 6 M H_2SO_4 to stop the reaction. Second, the suspension was magnetically separated and 60 μL of the supernatant was used for quantification in UV-vis measurements at 460 nm. For the specificity evaluation, H_2O_2 was replaced by ascorbic acid, L-cysteine, L-aspartic acid, L-proline, L-glycine and urea, respectively.

Optical detection of glucose in wine samples The white grape wine, J.J.Muller wine (Jerry Moselle, Germany), was bought from a local supermarket (Hangzhou, China). For glucose assay, the calibration plot was obtained first. The detection procedures are similar to that for H_2O_2 except that the addition of 30 μL of H_2O_2 was replaced by the addition of the mixture of 15 μL of 0.6 mg·mL^{-1} glucose oxidase and 15 μL of glucose of different concentrations (n = 3). For the detection of glucose in wine samples, the procedures were the same to the assay of glucose except replacing the addition of 15 μL glucose solutions by 15 μL of wine samples (n = 3).

Immobilization of ChOx MNP@Au-PB suspensions were diluted 10-fold with 0.1 M phosphate buffer (pH = 6.0, 50 μL), which were then mixed with 50 μL of ChOx (1 mg mL^{-1}) and kept at 4 °C for 1 h. Afterwards, the mixtures were magnetically separated and washed with 0.1 M phosphate buffer (pH = 6.0, 50 μL) for three times, and the supernatants were collected for the quantification using UV-vis spectroscopy at 280 nm. The mixtures of 50 μL of 0.1 M phosphate buffer (pH = 6.0) and 50 μL of ChOx (1 mg mL^{-1}) were adopted as the control and treated similarly, followed by the quantification of ChOx in supernatants using the same method. The immobilization rate was calculated as the rate of the absorbance of ChOx in the MNP@Au-PB case to that of the control. For comparison, the immobilization rates of ChOx in MNPs, MNP@PB and MNP@Au cases were also obtained using the same method.

Results and discussion

Characterization of MNP@Au-PB

We inspected the preparation of the MNP@Au-PB nanocomposites through digital imaging, as shown in Table S1 (please see detailed description in ESM). Because the preparation involved a series of precursors, we thus mixed some precursors to investigate the mechanism. The mixture of $NaAuCl_4$ and NH_2OH (sample 2) presented colorless, because NH_2OH was not able to reduce $NaAuCl_4$ solely [6]. In contrast, the presence of MNPs led to the production of MNP@Au (sample

3) [6]. The reason was that the reduction of $NaAuCl_4$ by NH_2OH was catalyzed by the nucleating effect from MNPs [6]. The mixing of MNPs, HCl and $K_4Fe(CN)_6$ (sample 4) led to rapid appearance of plenty of blue PB products, as illustrated as the Path 1 in Scheme 1. The mixture of $NaAuCl_4$, NH_2OH, $K_4Fe(CN)_6$ and HCl (sample 6) slowly turned to light blue due to the formation of PB-like $KFex[Au(CN)_2]y$ compounds [35]. Finally, the mixture of MNPs, $NaAuCl_4$, NH_2OH, $K_4Fe(CN)_6$ and HCl (sample 7) rapidly showed blue-light-green color, indicating the co-existing of PB and PB-like $KFex[Au(CN)_2]y$ compounds. The PB-like $KFex[Au(CN)_2]y$ were generated in solution while Au-PB was on the surface of MNPs (proximity effect). Hence, one can readily purify the MNP@Au-PB nanocomposites by magnetic separation (sample 9). In a magnetic field, MNP@Au-PB nanocomposites were rapidly collected leaving the supernatant totally clear, indicating the MNPs core and the magnetic property were well retained even after the self-sacrificing. It should guarantee the magnetic operability for applications.

SEM and TEM were further used to characterize the morphology of MNP@Au-PB, as shown in Fig. 1. The bare MNPs presented as nano-spheres (images a and c), and the MNP@Au-PB showed sphere-like clusters of cubes with whole size of 258 ± 56 nm ($n = 25$) (images b and d). According to previous report, these cubes were PB crystals [36]. Imaginably, the core surrounded by PB crystals should be the residual MNPs. Moreover, FTIR and XPS were adopted to characterize MNP@Au-PB in order to verify the composition of MNP@Au-PB (Fig. S1). As shown in Fig. S1a for FTIR, the bands of CN group, M-CN-M′ and Fe-O bond indicated the contents of PB and Fe_3O_4 [10]. As shown in Fig. S1b for the XPS results, the peaks of Fe (725.1 eV and 710.1 eV for Fe $2p_{1/2}$ and Fe $2p_{3/2}$, respectively), C (284 eV), N (397.8 eV), and O (530.1 eV) represented the presence of Fe_3O_4 and PB in both MNP@Au-PB and MNP@PB [37, 38]. Specially for MNP@Au-PB, two doublet peaks are observed with maxima at 84.1 eV and 88.1 eV, which are assigned to the $4f_{7/2}$ and $4f_{5/2}$ core levels of Au^0, indicating the presence of Au [39, 40].

To further determine the components of the nanocomposites, electrochemical tests using CV were conducted as shown in Fig. 2. MNP@Au-PB nanocomposites were modified onto the Au electrodes through casting-coat method, and then CV was collected in 0.1 M pH 6.0 phosphate buffer. For comparison, PB modified Au electrode prepared through conventional electrochemical deposition method was also tested similarly. As shown in Fig. 2a, the classic redox peaks of PB modified electrode are located at 0.19 V/0.13 V (PB and PW) and ca. 0.95 V/0.81 V (Berlin green/PB) [34]. For the MNP@Au-PB modified electrode, similar redox peaks at 0.19 V/0.13 V are found, as well as a oxidation peak of much higher intensity starting from 0.8 V and two reduction peaks at 0.81 V and 0.6 V. Here, these peaks appear on account of two pairs of redox reactions namely, the pairs of Berlin green/PB (ca. 0.95 V/0.81 V) and Au oxide/Au (ca. 1.0 V/0.6 V), which share the oxidation peak zoom, demonstrating the presence of PB and Au again. Moreover, a new oxidation peak also arises at 0.47 V, which is ascribed to the oxidation of Fe^{2+} to

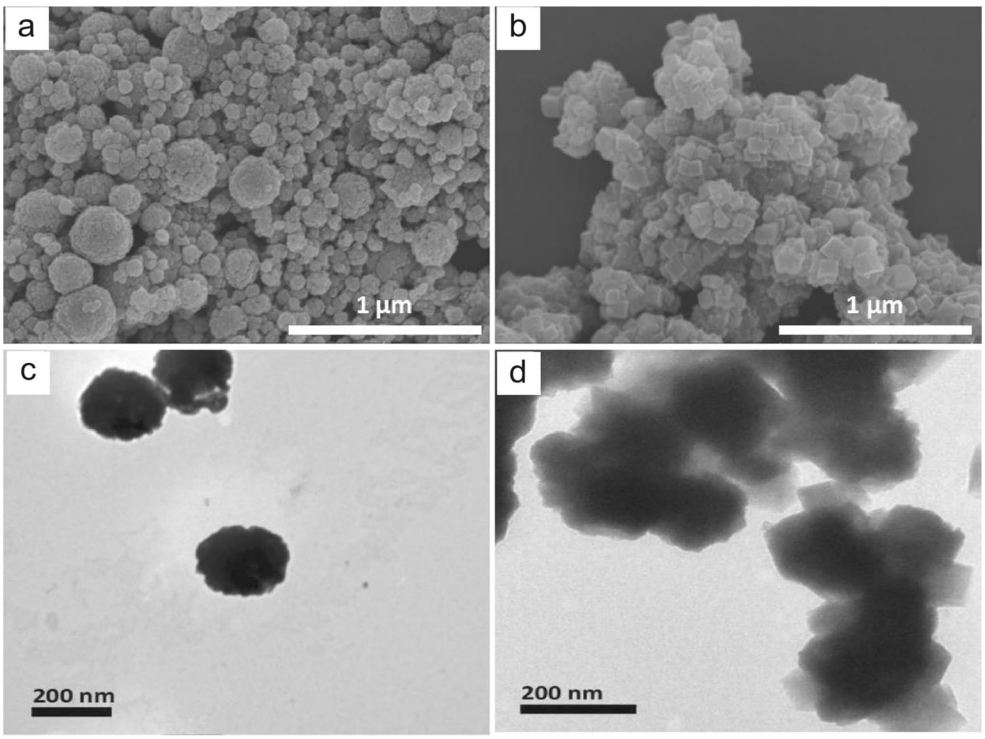

Fig. 1 SEM and TEM images of MNPs (a and c) and MNP@Au-PB (b and d)

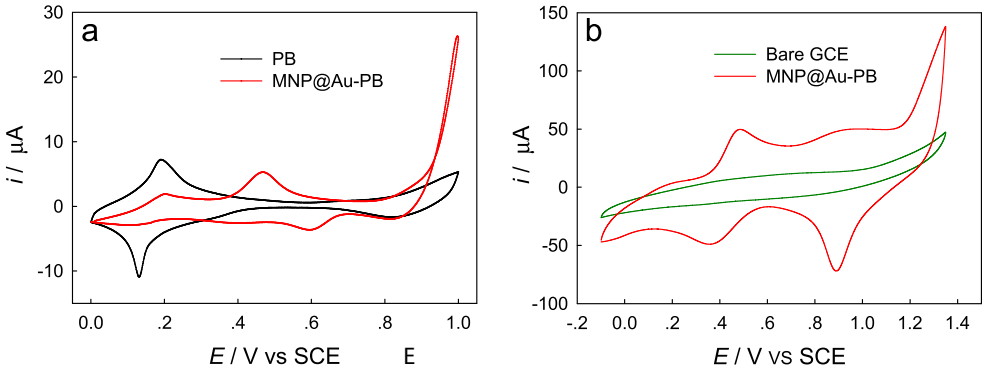

Fig. 2 **(a)** CV curves of PB and MNP@Au-PB modified Au electrodes in pH 6.0 phosphate buffer; **(b)** CV curves of the bare GCE and alkaline-treated MNP@Au-PB/GCE electrode in solution containing 0.1 M H_2SO_4 and 0.1 M K_2SO_4. Scan rate: 0.05 V s^{-1}

Fe^{3+} in Fe_3O_4, proving the presence of MNPs again. Furthermore, to more solidly prove the presence of Au, MNP@Au-PB modified glass carbon electrodes (GCE) were prepared similarly and then treated with NaOH to remove PB but retain Au. The mechanism is that PB can be readily degraded in alkaline solution. Then, CV of the electrode in a solution containing 0.1 M H_2SO_4 was collected (Fig. 2b). Clearly, in the absence of PB, no related peaks are observed, and the pair of redox peaks of Au oxide/Au are found starting at around 1.2 V and 0.9 V, respectively, proving the existence of Au component again.

Electrochemical detection of H_2O_2

To investigate the catalysis performance of MNP@Au-PB, the nanocomposites were modified on Au electrodes and then the electrochemical catalysis ability to H_2O_2 was examined using potentiostatic method, as shown in Fig. 3a. For comparison, MNPs, MNP@Au and MNP@PB modified Au electrodes were also prepared (with the same concentration of MNPs) and tested. The MNPs and MNP@Au modified electrodes gave current responses of 0.20 ± 0.02 μA ($n = 3$, same as below) and 0.41 ± 0.03 μA, respectively. In contrast, the MNP@PB modified electrodes presented significantly enhanced responses up to 12.9 ± 0.9 μA, due to the high catalysis ability of PB component. Surprisingly, the MNP@Au-PB modified electrodes, furthermore, promoted the responses to 21.6 ± 1.2 μA, which is 1.7 folds of that of MNP@PB. The reason should be the incorporation of Au that can enhance the conductivity of the nanocomposites. This result also highlights the advantages of the dual-function shell structure.

Based on the high catalysis ability of MNP@Au-PB, we further used the modified electrodes for the electrochemical detection of H_2O_2 by potentiostatic method at −0.05 V in 0.1 M phosphate buffer (pH 6.0). As shown in Fig. 3b, the current increases along with the addition of H_2O_2 and stabilizes within 5 s. The sensor exhibits a sensitivity of 0.738 μA cm^{-2} μM^{-1}, a linear detection range (LDR) from 4.0 μM to 22.12 mM and a limit of detection (LOD) of 1.1 μM ($S/N = 3$). Compared with some H_2O_2 sensors reported (Table S2), performance of the sensor is comparable to or better than most of analogues. The high performance should be the contribution of strong catalysis ability of PB and the synergetic effect from Au.

Colorimetric detection of H_2O_2

To further explore the application of the MNP@Au-PB nanocomposites, an optical colorimetric sensing strategy was developed. Briefly, MNP@Au-PB was mixed with TMB and H_2O_2 of given concentration, then the mixture was kept undisturbed for 10 min. After the reaction was stopped using

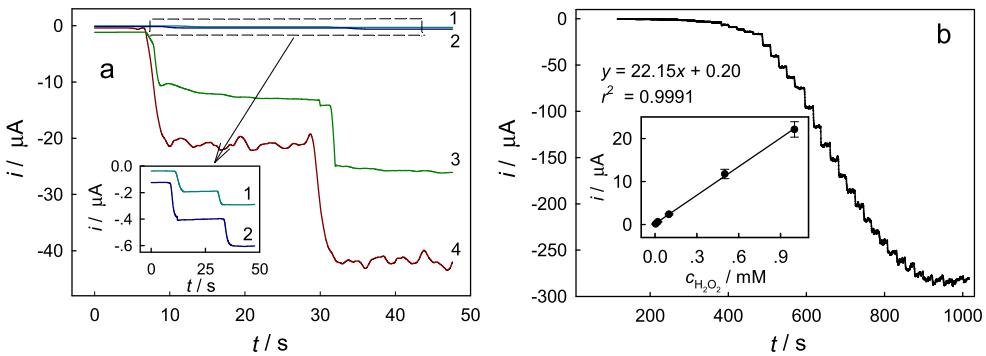

Fig. 3 **(a)** Chronoamperometric responses of the MNPs (1), MNP@Au (2), MNP@PB (3) and MNP@Au-PB (4) modified Au electrodes to 1 mM H_2O_2 at −0.05 V in pH 6.0 phosphate buffer. **(b)** Chronoamperometric responses of MNP@Au-PB modified Au electrodes to successive additions of H_2O_2 at −0.05 V in pH 6.0 phosphate buffer and the corresponding calibration plot

H_2SO_4, UV-vis spectra were collected finally. During the detection, PB catalyzed H_2O_2 and simultaneously oxidized TMB to its oxide (blue in color), which turned to yellow in the strong acidic solution. Therefore, the response signal was collected using UV-vis spectra at 460 nm. As shown in Fig. 4a, along with the increase of the concentration of H_2O_2, the final solutions gradually turned deepened yellow (the inserted image), and the absorption intensities at 460 nm also gradually increased. The phenomena indicate the catalysis of TMB to its oxide by the MNP@Au-PB in the presence of H_2O_2. The colorimetric sensor exhibits LDR from 5.0 μM to 5.0 mM with LOD at 1.27 μM ($S/N = 3$), which is equal to that of electrochemical sensor. These results highlight again the high performance of MNP@Au-PB and the potential for sensing applications.

Reversibility and selectivity

During the catalysis process, PB played a role mimic to HRP. Briefly, PB catalyzed the reduction of H_2O_2 and turned themselves to the oxidative form. While the co-existing TMB turned the oxidative form of PB to reductive one that was capable to catalyze H_2O_2 again. Therefore, the catalysis ability of MNP@Au-PB was reversible. Moreover, the reusability of the nanocomposites was examined. Briefly, after one detection, the nanocomposites were collected using magnet and then used for another round of detection. After five rounds of detections, the responses ($n = 3$) were still (95 ± 1) % of the initials. This should prove the nanocomposites are capable for repeated detections.

To investigate the selectivity of MNP@Au-PB-based sensor, some interferences, including ascorbic acid, urea, L-Cysteine, L-Aspartic acid, L-Glycine and L-Proline, were chosen for comparison. The results are shown in Fig. S2. Briefly, the intensity of the absorption peak at 460 nm of 500 μM H_2O_2 was compared with the those of ultrapure water (control experiment), 1 mM ascorbic acid, 1 mM urea, 1 mM L-Cysteine, 1 mM L-Aspartic acid, 1 mM L-Glycine and 1 mM L-Proline. All above interferences exhibited responses lower than 6.0% of that of H_2O_2, indicating good selectivity. Because a key procedure of the colorimetric detection is the oxidation of TMB to its oxide, general interferences lack of oxidation ability have minor influence on the detection.

Detection of glucose in wine samples

The feasibility of the sensor for real application was examined by applying for the detection of glucose in wine. Glucose was catalyzed by glucose oxidase to generate H_2O_2, which then was detected using the sensor. The value of adsorption peak at 460 nm were collected for quantification. Firstly, we obtained the calibration plot for the detection of glucose in 0.1 M phosphate buffer (pH 6.0). As shown in Fig. S3, the linear detection range was from 10.0 μM to 500.0 μM. Then the white grape wine, whose glucose content is 28.58 mM as determined by a standard high performance liquid chromatography method [41], was diluted for the real sample detection. The concentration detected by the sensor was 29.89 ± 2.9 mM. The relative standard deviation is 104.6%. Above results should prove that the sensor is feasible for real sample detection.

Immobilization of ChOx

The construction of dual-functional shell has gifted the advantage of synergetic catalysis to enhance the sensing performance. Here, another merit of this structure was exploited for biosensing. As mentioned before, PB is powerful for catalysis, however, its surficial property for immobilization of other species is poor [26]. Therefore, the incorporation of Au, which is a type of commonly adopted matrix material for

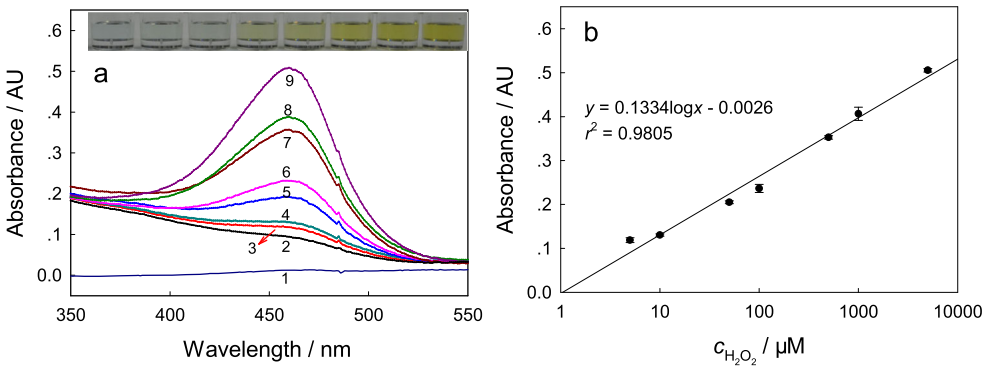

Fig. 4 **(a)** UV-vis spectra of the final supernatants of the mixture of TMB and 1 mM H_2O_2 (1), as well as the supernatants for the detection of different concentrations of H_2O_2: 0 (2), 5 μM (3), 10 μM (4), 50 μM (5), 100 μM (6), 500 μM (7), 1 mM (8) and 5 mM (9) (the insert shows the digital picture of MNP@Au-PB suspensions after the detections, samples from left to right are presented corresponding to above concentrations). **(b)** The absorption peaks at 460 nm were adopted for calculation to obtain the calibration plot ($n = 3$)

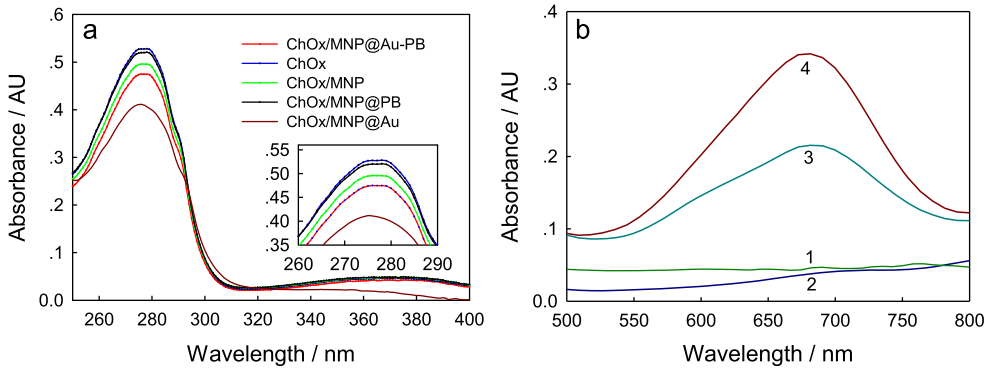

Fig. 5 **(a)** UV-vis spectra of the supernatants of the mixtures (1 h) of MNP/ChOx, MNP@PB/ChOx, MNP@Au-PB/ChOx, MNP@Au/ChOx and ChOx. **(b)** UV-vis spectra of supernatants of ChOx (1), MNP/ChOx (2), MNP@PB/ChOx (3) and MNP@Au-PB/ChOx (4) after the incubation (10 min) with 10 mM TMB and 100 mM choline chloride in pH 6.0 phosphate buffer

immobilization, should gift the enhanced immobilization ability. To evaluate the speculation, MNPs, MNP@PB, MNP@Au and MNP@Au-PB were exposed to enzyme ChOx and then the immobilization amounts were obtained using UV-vis spectroscopy. Briefly, MNPs or MNP composites were incubated with ChOx and then magnetically separated, while the supernatants were collected for UV-vis spectroscopy measurements at 280 nm. As a control, ChOx solution with the same concentration as the added for immobilization was treated with the same procedures, and then the UV-vis spectra were also collected. Therefore, the decrease of the peak intensity comparing to original ChOx solution was approximately transferred to be the amount immobilized. Finally, the immobilization capability was calculated as the ratio of immobilized ChOx in mg to the MNPs or MNP composites in g. As shown in Fig. 5a, the adsorption of ChOx on MNP@PB (162 ± 15 mg g^{-1}) decreased to be 38% of that on MNPs (429 ± 38 mg g^{-1}), highlighting the poor immobilization ability of PB. On the other hand, MNP@Au nanocomposites exhibited adsorbability of 813 ± 95 mg g^{-1}, indicating the significant enhancement of adsorption due to the Au shell. The incorporation of Au (MNP@Au-PB) thus made the adsorption amount (593 ± 61 mg g^{-1}) 1.38 fold of that on MNPs. Therefore, MNP@Au-PB nanocomposites integrate the catalysis ability of PB and immobilization ability of Au, thus should contribute as multi-functional biosensing platform.

For a state-of-concept application, we further examined and compared the biosensing abilities of MNPs, MNP@PB and MNP@Au-PB to choline using the colorimetric method. After the modification of ChOx on above three matrices, TMB and choline were added to trigger the catalysis cascade. Namely, ChOx catalyzed choline to generate H_2O_2, which was catalyzed by peroxidase-like PB to make TMB turn to its oxide (blue in color). Finally, the supernatants after the magnetic separation were collected for UV-vis spectroscopy measurements at 650 nm, as shown in Fig. 5b. Clearly, the efficiency of the enzyme catalysis cascade should be determined by the amount of ChOx and the catalysis ability of the peroxidase-like analogues. As the control, the ChOx solution itself can not finish the catalysis cascade in the absence of PB, thus gave no absorption peak. Similarly, although the MNP/ChOx have good ChOx immobilized and MNPs themselves play a little role as peroxidase, the absence of PB led to very small absorption peak. In contrast, although MNP@PB/ChOx had less ChOx than MNP@ChOx, the strong catalysis ability of PB shell gifted a complete enzyme catalysis cascade, giving a strong peak. Imaginably, the MNP@Au-PB contributed the strongest adsorption peak, which is 1.62 fold of that of MNP@PB, due to the increased ChOx immobilization. Again, this result highlights the superiority of the dual-function shell and promising prospect of MNP@Au-PB for biosensing applications.

Conclusions

In summary, a self-sacrificing-catalyzing method has been developed to prepare MNP@Au-PB core@dual-functional-shell nanocomposites. The nanocomposites exhibit inherent magnetic property from the core for magnetic operations, and integrate the peroxidase-like catalysis ability of PB and enhanced conductivity from Au, exhibiting sensing performances comparable with or better than most of analogues. Furthermore, the incorporation of Au also gifts the nanocomposites with the superiority to immobilize ChOx for biosensing. The MNP@Au-PB should be promising in catalysis and sensing/biosensing fields, and the self-sacrificing-catalyzing method might open new avenue for preparation of multi-functional nanocomposites. However, because PB is inherently susceptive to alkali, so alkaline solutions should be avoided. Moreover, appropriate block of the surface of the nanocomposites should be conducted to avoid interferences prior to the application in complex samples. Therefore, further efforts are needed to make the nanocomposites more robust.

Acknowledgements This work was supported by National Natural Science Foundation of China (Grants 21505120, 21775137), and the State Key Laboratory of Chemo/Biosensing and Chemometrics.

Compliance with ethical standards

The author(s) declare that they have no competing interests.

References

1. Urbanova V, Magro M, Gedanken A, Baratella D, Vianello F, Zboril R (2014) Nanocrystalline Iron oxides, composites, and related materials as a platform for electrochemical, magnetic, and chemical biosensors. Chem Mater 26(23):6653–6673. https://doi.org/10.1021/cm500364x
2. Tuček J, Kemp KC, Kim KS, Zbořil R (2014) Iron-oxide-supported Nanocarbon in lithium-ion batteries, medical, catalytic, and environmental applications. ACS Nano 8 (8):7571–7612. doi:https://doi.org/10.1021/nn501836x
3. Wu L, Mendoza-Garcia A, Li Q, Sun S (2016) Organic phase syntheses of magnetic nanoparticles and their applications. Chem Rev 116(18):10473–10512. https://doi.org/10.1021/acs.chemrev.5b00687
4. Gao J, Gu H, Xu B (2009) Multifunctional magnetic nanoparticles: design, synthesis, and biomedical applications. Acc Chem Res 42(8):1097–1107. https://doi.org/10.1021/ar9000026
5. Xiao D, Lu T, Zeng R, Bi Y (2016) Preparation and highlighted applications of magnetic microparticles and nanoparticles: a review on recent advances. Microchim Acta 183(10):2655–2675. https://doi.org/10.1007/s00604-016-1928-y
6. Zou C, Fu Y, Xie Q, Yao S (2010) High-performance glucose amperometric biosensor based on magnetic polymeric bionanocomposites. Biosens Bioelectron 25(6):1277–1282. https://doi.org/10.1016/j.bios.2009.10.014
7. Zhang Q, Li L, Qiao Z, Lei C, Fu Y, Xie Q, Yao S, Li Y, Ying Y (2017) Electrochemical conversion of Fe_3O_4 magnetic nanoparticles to electroactive Prussian blue analogues for self-sacrificial label biosensing of avian influenza virus H5N1. Anal Chem 89(22): 12145–12151. https://doi.org/10.1021/acs.analchem.7b02784
8. Bordage Al, Moulin R, Fonda E, Fornasieri G, RiviÃre E, Bleuzen A (2018) Evidence of the Core–Shell Structure of (Photo)magnetic CoFe Prussian Blue Analogue Nanoparticles and Peculiar Behavior of the Surface Species Journal of the American Chemical Society 140 (32):10332–10343. doi: https://doi.org/10.1021/jacs.8b06147
9. Fu G, Liu W, Li Y, Jin Y, Jiang L, Liang X, Feng S, Dai Z (2014) Magnetic Prussian blue nanoparticles for targeted Photothermal therapy under magnetic resonance imaging guidance. Bioconjug Chem 25(9):1655–1663. https://doi.org/10.1021/bc500279w
10. Zhao G, Feng J-J, Zhang Q-L, Li S-P, Chen H-Y (2005) Synthesis and characterization of Prussian blue modified magnetite nanoparticles and its application to the Electrocatalytic reduction of H_2O_2. Chem Mater 17(12):3154–3159. https://doi.org/10.1021/cm048078s
11. Ma Y, Xu G, Wei F, Cen Y, Xu X, Shi M, Cheng X, Chai Y, Sohail M, Hu Q (2018) One-pot synthesis of a magnetic, Ratiometric fluorescent Nanoprobe by encapsulating Fe_3O_4 magnetic nanoparticles and dual-emissive rhodamine B modified carbon dots in metal–organic framework for enhanced HClO sensing. ACS Appl Mater Interfaces 10 (24):20801–20805. doi:https://doi.org/10.1021/acsami.8b05643
12. Sadiq MM, Li H, Hill AJ, Falcaro P, Hill MR, Suzuki K (2016) Magnetic induction swing adsorption: an energy efficient route to porous adsorbent regeneration. Chem Mater 28(17):6219–6226. https://doi.org/10.1021/acs.chemmater.6b02409
13. Chen Y, Xiong Z, Peng L, Gan Y, Zhao Y, Shen J, Qian J, Zhang L, Zhang W (2015) Facile preparation of Core–Shell magnetic metal–organic framework nanoparticles for the selective capture of Phosphopeptides. ACS Appl Mater Interfaces 7 (30):16338–16347. doi:https://doi.org/10.1021/acsami.5b03335
14. Kobayashi H, Mitsuka Y, Kitagawa H (2016) Metal nanoparticles covered with a metal–organic framework: from one-pot synthetic methods to synergistic energy storage and conversion functions. Inorg Chem 55 (15):7301–7310. doi:https://doi.org/10.1021/acs.inorgchem.6b00911
15. Chen L, Li H, Zhan W, Cao Z, Chen J, Jiang Q, Jiang Y, Xie Z, Kuang Q, Zheng L (2016) Controlled encapsulation of flower-like Rh–Ni alloys with MOFs via tunable template Dealloying for enhanced selective hydrogenation of alkyne. ACS Appl Mater Interfaces 8 (45):31059–31066. doi:https://doi.org/10.1021/acsami.6b11567
16. Fu Y, Callaway Z, Lum J, Wang R, Lin J, Li Y (2014) Exploiting enzyme catalysis in ultra-low ion strength Media for Impedance Biosensing of avian influenza virus using a bare interdigitated electrode. Anal Chem 86(4):1965–1971. https://doi.org/10.1021/ac402550f
17. Afkhami A, Shirzadmehr A, Madrakian T, Bagheri H (2014) Improvement in the performance of a Pb^{2+} selective potentiometric sensor using modified core/shell SiO_2/Fe_3O_4 nano-structure. J Mol Liq 199:108–114. https://doi.org/10.1016/j.talanta.2012.03.066
18. Bagheri H, Afkhami A, Sabertehrani M, Khoshsafar H (2012) Preparation and characterization of magnetic nanocomposite of Schiff base/silica/magnetite as a preconcentration phase for the trace determination of heavy metal ions in water, food and biological samples using atomic absorption spectrometry. Talanta 97:87–95. https://doi.org/10.1016/j.talanta.2012.03.066
19. Bagheri H, Asgharinezhad AA, Ebrahimzadeh H (2016) Determination of trace amounts of Cd(II), Cu(II), and Ni(II) in food samples using a novel functionalized magnetic Nanosorbent. Food Anal Methods 9(4):876–888. https://doi.org/10.1007/s12161-015-0264-x
20. Bagheri H, Yamini Y, Safari M, Asiabi H, Karimi M, Heydari A (2016) Simultaneous determination of pyrethroids residues in fruit and vegetable samples via supercritical fluid extraction coupled with magnetic solid phase extraction followed by HPLC-UV. J Supercrit Fluids 107:571–580. https://doi.org/10.1007/s12161-015-0264-x
21. Bagheri H, Pajooheshpour N, Afkhami A, Khoshsafar H (2016) Fabrication of a novel electrochemical sensing platform based on a core–shell nano-structured/molecularly imprinted polymer for sensitive and selective determination of ephedrine. RSC Adv 6(56):51135–51145. https://doi.org/10.1039/C6RA09488K
22. Yin PT, Pongkulapa T, Cho H-Y, Han J, Pasquale NJ, Rabie H, Kim J-H, Choi J-W, Lee K-B (2018) Overcoming Chemoresistance in Cancer via combined MicroRNA therapeutics with anticancer drugs using multifunctional magnetic Core–Shell nanoparticles. ACS Appl Mater Interfaces 10 (32):26954–26963. doi:https://doi.org/10.1021/acsami.8b09086
23. Zirak M, Garegeshlagi EJ (2018) Picolinimidoamide-cu(II) complex anchored on Fe_3O_4@SiO_2 core-shell magnetic nanoparticles: an efficient reusable catalyst for click reaction. J Coord Chem 71(8):1168–1179. https://doi.org/10.1080/00958972.2018.1450975
24. Moorthy MS, Subramanian B, Panchanathan M, Mondal S, Kim H, Lee KD, Oh J (2017) Fucoidan-coated core-shell magnetic mesoporous silica nanoparticles for chemotherapy and magnetic hyperthermia-based thermal therapy applications. New J Chem 41(24):15334–15346. https://doi.org/10.1039/c7nj03211k
25. Hegazy M, Zhou P, Wu G, Wang L, Rahoui N, Taloub N, Huang X, Huang Y (2017) Construction of polymer coated core-shell

magnetic mesoporous silica nanoparticles with triple responsive drug delivery. Polym Chem 8(38):5852–5864. https://doi.org/10.1039/c7py01179b

26. Sun L, Li Q, Hou M, Gao Y, Yang R, Zhang L, Xu Z, Kang Y, Xue P (2018) Light-activatable Chlorin e6 (Ce6)-imbedded erythrocyte membrane vesicles camouflaged Prussian blue nanoparticles for synergistic photothermal and photodynamic therapies of cancer. Biomater Sci 6(11):2881–2895. https://doi.org/10.1039/C8BM00812D
27. Wang T, Fu Y, Chai L, Chao L, Bu L, Meng Y, Chen C, Ma M, Xie Q, Yao S (2014) Filling carbon nanotubes with Prussian blue nanoparticles of high peroxidase- like catalytic activity for colorimetric Chemoand biosensing. Chem Eur J 20(9):2623–2630. https://doi.org/10.1002/chem.201304035
28. Wang T, Fu Y, Bu L, Qin C, Meng Y, Chen C, Ma M, Xie Q, Yao S (2012) Facile synthesis of Prussian blue-filled multiwalled carbon nanotubes nanocomposites: exploring filling/electrochemistry/mass-transfer in Nanochannels and cooperative biosensing mode. J Phys Chem C 116(39):20908–20917. https://doi.org/10.1021/jp306492a
29. Farka Z, Čunderlová V, Horáčková V, Pastucha M, Mikušová Z, Hlaváček A, Skládal P (2018) Prussian blue nanoparticles as a catalytic label in a Sandwich Nanozyme-linked immunosorbent assay. Anal Chem 90 (3):2348–2354. doi:https://doi.org/10.1021/acs.analchem.7b04883
30. Jiang Y, Wang W, Li X, Wang X, Zhou J, Mu X (2013) Enzyme-mimetic catalyst-modified Nanoporous SiO_2 cellulose hybrid composites with high specific surface area for rapid H_2O_2 detection. ACS Appl Mater Interfaces 5 (6):1913–1916. doi:https://doi.org/10.1021/am400253d
31. Huang J, Zhu Y, Zhong H, Yang X, Li C (2014) Dispersed CuO nanoparticles on a silicon nanowire for improved performance of nonenzymatic H_2O_2 detection. ACS Appl Mater Interfaces 6(10):7055–7062. https://doi.org/10.1021/am501799w
32. Zhang Y, Bai X, Wang X, Shiu K-K, Zhu Y, Jiang H (2014) Highly sensitive Graphene–Pt nanocomposites Amperometric biosensor and its application in living cell H_2O_2 detection. Anal Chem 86 (19):9459–9465. doi:https://doi.org/10.1021/ac5009699
33. Song M, Wang J, Chen B, Wang L (2017) A facile, nonreactive hydrogen peroxide (H_2O_2) detection method enabled by ion chromatography with UV detector. Anal Chem 89(21):11537–11544. https://doi.org/10.1021/acs.analchem.7b02831
34. Deng C, Li M, Xie Q, Liu M, Tan Y, Xu X, Yao S (2006) New glucose biosensor based on a poly(o-phenylendiamine)/glucose oxidase-glutaraldehyde/Prussian blue/au electrode with QCM monitoring of various electrode-surface modifications. Anal Chim Acta 557(1):85–94. https://doi.org/10.1016/j.aca.2005.10.009
35. Harish S, Joseph J, Phani KLN (2011) Interaction between gold (III) chloride and potassium hexacyanoferrate (II/III)—does it lead to gold analogue of Prussian blue? Electrochim Acta 56(16):5717–5721. https://doi.org/10.1016/j.electacta.2011.04.044
36. Jiang Y, Yu S, Wang B, Li Y, Sun W, Lu Y, Yan M, Song B, Dou S (2016) Prussian blue@C composite as an ultrahigh-rate and long-life sodium-ion battery cathode. Adv Funct Mater 26(29):5315–5321. https://doi.org/10.1002/adfm.201600747
37. C. Carvalho CL, B. Silva AT, Luz RAS, Castro GMB, da Luz Lima C, Mastelaro VR, da Silva RR, Oliveira ON, CantanhÃªde W (2018) Development of $Co_3[Co(CN)_6]_2/Fe_3O_4$ Bifunctional Nanocomposite for Clinical Sensor Applications. ACS Appl Nano Mater:https://doi.org/10.1021/acsanm.1028b01106. doi:https://doi.org/10.1021/acsanm.8b01106
38. Ma S, Zhan S, Jia Y, Zhou Q (2015) Superior antibacterial activity of Fe_3O_4-TiO_2 Nanosheets under solar light. ACS Appl Mater Interfaces 7(39):21875–21883. https://doi.org/10.1021/acsami.5b06264
39. Bratescu MA, Cho S-P, Takai O, Saito N (2011) Size-controlled gold nanoparticles synthesized in solution plasma. J Phys Chem C 115(50):24569–24576. https://doi.org/10.1021/jp207447c
40. Ono LK, Roldan Cuenya B (2008) Formation and thermal stability of Au_2O_3 on gold nanoparticles: size and support effects. J Phys Chem C 112(12):4676–4686. https://doi.org/10.1021/jp711277u
41. Dai H, Li Y, Zhang Q, Fu Y, Li Y (2018) A colorimetric biosensor based on enzyme-catalysis-induced production of inorganic nanoparticles for sensitive detection of glucose in white grape wine. RSC Adv 8(59):33960–33967. https://doi.org/10.1039/C8RA06347H